Acetylation of RORβ by histone acetyltransferase p300 and deacetylation by SIRT1 modulates receptor stability, turnover and transcriptional activity.

Timothy O'Leary[1], Denis Shutin[1], Dean P. Edwards[2], Patrick R. Griffin[1]* and Mi Ra Chang[1]*

[1]Department of Molecular Medicine, The Herbert Wertheim UF Scripps Institute for Biomedical Innovation & Technology, Jupiter, FL 33458

[2]Department of Molecular and Cellular Biology, Baylor College of Medicine, Houston, TX 77030 USA.

Short title: RORβ is regulated by p300 and SIRT1.

* Correspondence should be addressed to pgriffin2@ufl.edu and mirachang@ufl.edu

Graphical Abstract:

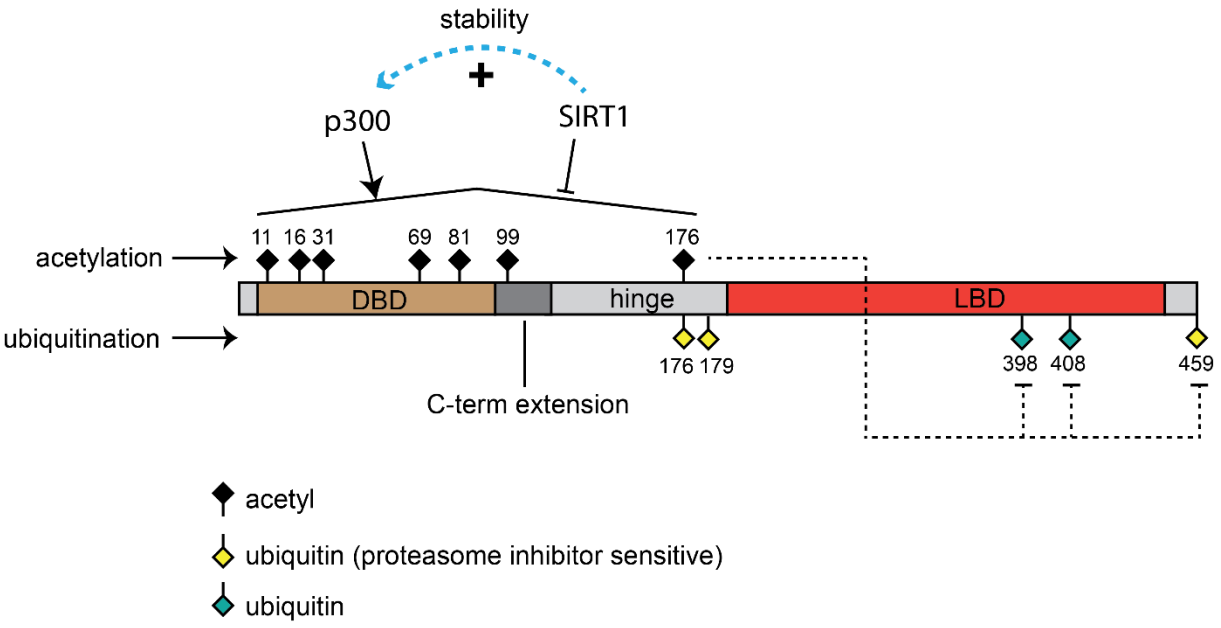

Abstract

RORβ is an understudied nuclear receptor recently implicated in numerous pathologies. Using immunoprecipitation mass spectrometry, the transcription factor coregulatory protein and histone acetyltransferase p300 (*EP300*) was identified as a direct interacting protein of RORβ. Crosslinking mass spectrometry (XL-MS) confirmed that p300 interacts with the DNA binding domain (DBD), hinge region, and ligand binding domain (LBD) of RORβ. Both p300 and SIRT1 impact the turnover rate and transcriptional activity of RORβ. p300-dependent acetylation sites were found to be constrained to the DBD and hinge region of RORβ and were deacetylated by SIRT1. Sites that were ubiquitinated in the presence of p300 and SIRT1 were also discovered, with some sites sensitive to proteasome inhibitor. A constitutively acetylated mimic at K176 in the hinge prevented ubiquitination of RORβ at distal sites. Uncovering regulatory mechanisms of RORβ via protein interactions and PTMs will provide strategies for development of therapeutics targeting the receptor.

Teaser: p300 and SIRT1 work in concert to coordinate posttranslational modifications of the nuclear receptor RORβ.

Introduction

The nuclear receptor (NR) superfamily of ligand regulated transcription factors has proven to be a rich source of targets for the development of therapeutics for a wide range of human diseases. Endogenous small molecule regulation of these proteins control processes central to most aspects of mammalian physiology. The retinoic acid receptor-related orphan receptors (RORs) are members of the NR1F subfamily of NRs that play regulatory roles in the maintenance of a variety of physiological and pathological processes including regulation of glucose and lipid metabolism, bone homeostasis, circadian rhythms, cancer, immune functions, and neurological disorders (*1-6*). The ROR subfamily, which has amino acid sequence homology to both the retinoic acid receptors (RARs) and the retinoid X receptors (RXRs), includes three major isoforms; RORα, RORβ, and RORγ (*7*). However, unlike the RARs and RXRs which are modulated by retinoids, the activity of the RORα and RORγ is modulated endogenously by oxysterols and other cholesterol metabolites (*8-10*). Interestingly, although RORβ can bind oxysterols, the activity of the receptor can be antagonized by binding all trans retinoic acid (ATRA), although it is not clear if ATRA is its endogenous ligand (*11, 12*). The physiological functions of RORα and RORγ have been well characterized, RORβ (NR1F2) has been significantly less well studied as the field has focused on development of RORα or RORγ-selective agonists and antagonists to modulate immune function as possible therapeutics for autoimmune disease and cancer (*7, 13*).

RORβ displays the general domain architecture observed within the NR superfamily consisting of a short but variable and unstructured N-terminal A/B domain that contains ligand-independent co-regulatory protein binding sites referred to as Activation Function-1 (AF-1). This domain is linked to a highly conserved two zinc finger DNA-binding domain (DBD; C domain) flanked by an unstructured D domain or hinge region that encodes part of the nuclear localization sequence (NLS). The hinge region is often a site for regulatory post-translational modifications, such as acetylation, SUMOylation, ubiquitination and phosphorylation (*14*). Hinge PTMs can impact various aspects of receptor function including protein folding and stability, transcriptional activity, and subcellular distribution. This phenomenon has been particularly well studied in the androgen receptor (*15*). This region connects to a ligand-binding domain (LBD; E domain) containing a ligand-dependent coregulator binding surface called AF-2 (*16*).

Previous studies suggest that expression of RORβ is limited primarily to the central nervous system, eyes, and bone (*17-19*). In the CNS, RORβ is involved in processing of sensory information, and regulation of circadian clock. RORα and RORβ have been implicated

in the pathology of diseases associated with dysregulation of the circadian rhythm including sleep disorders, bipolar disorder, and schizophrenia (*17, 18, 20-23*). Moreover, RORβ is associated with_Alzheimer's susceptibility in excitatory neurons (*24, 25*). RORβ is expressed in retinal progenitor cells during development and genetic deletion of RORβ results in retinal degeneration implicating its role in vision and RORβ null mice are born blind (*26*). More recently, it was shown that RORβ plays a role in osteogenesis by inhibiting Runx2 activity (*19*). The expression level of RORβ is inversely correlated with the osteogenic potential suggesting that activation of RORβ may drive suppression of osteoblast mineralization and it might reduce the osteoarthritis pathology (*19*). It was shown that RORβ and a subset of RORβ-regulated genes were increased in bone biopsies from post-menopausal women compared to pre-menopausal women suggesting a role for RORβ in human age-related bone loss (*27*). Additionally, it was shown that the miR-219a-5p regulates RORβ during osteoblast differentiation and in age-related bone loss (*28*). While RORβ$^{-/-}$ mice display bone abnormalities, it was shown that deletion of RORβ was osteoprotective (*29*). There are two isoforms of RORβ, β1 and β2, that differ in length of the N-termini as a result of alternative splicing. The focus here is on RORβ1, which is abbreviated to RORβ.

Given the important roles RORβ plays in physiology, it is surprising that the receptor's endogenous ligand, direct target genes, and coregulators have yet to be described. To help fill this void in knowledge, results presented demonstrate the coregulator and lysine acetyltransferase p300 binds directly to RORβ. Previously it has been shown that p300 can acetylate lysine residues of NRs leading to alterations in DNA binding affinity, receptor-protein interactions, receptor turnover, and susceptibility to PTMs such as SUMOylation, ubiquitination and phosphorylation (*30, 31*). Therefore, tandem mass spectrometry was employed to identify and quantify levels of acetylation at lysine residues within RORβ, as well as their sensitivity to sirtuin deacetylase activity. Acetylation of RORβ by p300 did not appear to influence DNA binding, therefore alternate explanations for the effect of p300 and SIRT1 were explored (*32*). Ubiquitination modification sites of RORβ were evaluated, revealing a subset of ubiquitination sites sensitive to proteasome inhibitor. SUMOylation was also implicated, with the presence of SIRT1 inducing a significant decrease in SUMO2 and related SUMOylation proteins immunoprecipitated with RORβ. Combined, the studies presented here suggest p300 and SIRT1 function in coordinating a regime of posttranslational modifications including acetylation, ubiquitination, and SUMOylation of RORβ to modulate receptor stability, turnover and transcriptional activity.

RESULTS

RORβ directly interacts with p300

To find potential interactors of RORβ we used a modified version of the protocol for rapid immunoprecipitation of endogenous proteins (RIME) (*33*). HA-RORβ or mock vector was transiently transfected into TC28a2 chondrocytes, and live cells were treated with formaldehyde for *in situ* crosslinking of chromatin complexes, and the nuclear lysate was immunoprecipitated with anti-HA beads. Co-immunoprecipitated proteins were identified by mass spectrometry and quantified using MS1-based label-free protein quantification. This yielded a set of proteins that were enriched in pulldowns from RORβ transfected cells and p300, a known nuclear receptor coregulator, was one of the top enriched proteins (**Fig. 1a**). There were 57 putative RORβ interactors with at least 5-fold increase in abundance relative to the negative control and with a p-value less than 0.05 (n=3), with 18 of these being involved in transcriptional regulation (**Fig. S1**). A heatmap comparing protein abundance in RORβ transfected to mock samples shows that RORβ was not found in the control sample (**Fig. 1b**). To reinforce p300 as an interactor of RORβ, p300 was pulled down using purified recombinant RORβ as bait. Lysate from HEK 293T cells transfected with p300 was incubated with nickel-displaying magnetic beads that had been pre-complexed with either His-RORβ in the presence of BSA or with BSA alone. Subsequent immunoblots for p300 showed greatly enhanced signal for the p300 band for pulldowns with His-RORβ complexed beads (**Fig. 1c**)**.**

The interaction between p300 and RORβ was further examined by *in vitro* crosslinking of full length RORβ with a truncated p300 acetyltransferase core containing the bromo, RING, and histone acetyltransferase (HAT) domains (amino acids 1040-1850 comprise the p300 core). Crosslinking was performed as described in the methods. SDS-PAGE analysis of the crosslinking reaction products showed the appearance of a band near 160 kDa, the sum of the molecular weights of the p300 core and RORβ, which did not appear in the vehicle treated control (**Fig. S2a**). Subsequent digestion and mass spectrometry analysis identified eight high confidence interprotein crosslinks. Six of the eight interprotein crosslinks bridged p300 and the RORβ DNA-binding domain (**Fig. 2a**). RORβ DBD residues K69, K81, and K88 formed six crosslinks with residues K1047, K1105, K1180, K1235, K1637 and K1812 from p300. The RING

domain of p300 also showed extensive crosslinking, and four of the eight interprotein crosslinks found on p300 originated from the RING domain. RING residues K1180 and K1235 crosslinked to RORβ residues in both the DBD and LBD. RORβ residue K69 crosslinked with p300 HAT residue K1637 as well as K1812 from the C-terminal side of the p300 HAT domain. RORβ residue K81 was crosslinked to p300 residues from the bromo domain (K1047). To visualize the crosslinking data in a structural context, an AlphaFold 3 model of the p300 core complex and RORβ was constructed, with RORβ bound to RORE DNA oligomer 5'-AGGTCA-3'. The interprotein crosslinks found by mass spectrometry were then mapped to an AlphaFold 3.0 model (**Fig. 2b**) This computational model suggests folding of the RORβ DBD and LBD domains about the hinge region, so that each are brought into proximity of the RING domain of p300. This aligns with a proposed mechanism where transcription factor interactions with the p300 RING domain led to exposure of the p300 HAT domain and autoactivation of p300 (*34*). The model also suggests that the C-terminal region of RORβ, which contains part of the AF2, interacts directly with p300. XL-MS was also performed with full length p300 and RORβ, which identified numerous crosslinks from p300 to the RORβ DBD. Additionally, two of the three NR-box motifs (LXXLL) in p300 were found to interact with the LBD. K336 of p300, near the LVLLL NR-box at 342-346, crosslinked to K221, K253, and K459 in the RORβ LBD, while p300 residue K2042 (LQNLL, 2051-2055) crosslinked with LBD residue K459 (**Fig. S2b**).

p300 effects RORβ protein abundance and acetylation

p300 is known to directly acetylate numerous transcription factors, including nuclear receptors (*14*). Acetylation of nuclear receptors by p300 is regulated by acetyl CoA, HDACs, and specifically the NAD+ dependent Sirtuins (e.g., SIRT1). Therefore, we assessed the effect of p300 on RORβ acetylation, first by immunoblotting for acetyl lysine and RORβ from lysates of HEK 293T cells transfected with RORβ +/- p300. In the absence of deacetylase inhibitor, acetylation of RORβ was increased in the presence of p300, and the addition of a sirtuin inhibitor (EX-527) significantly increased acetylation in the presence of p300 (**Fig. 3a**). Treatment with the sirtuin inhibitor EX-527 led to approximately eight-fold increase in acetyl lysine signal in p300 transfected samples compared to those transfected with RORβ alone. Immunoblotting for RORβ showed p300 increased the level of RORβ, which was doubled in the absence of deacetylase inhibitor (EX-527). Interestingly, while EX-527 showed an increase in RORβ acetylation, it dampened the effect of p300 on RORβ abundance. To determine whether this increase in RORβ was due to enhanced stabilization of RORβ by p300, we treated

RORβ+/- p300 transfected HEK 293T cells with cycloheximide (CHX) to inhibit new protein synthesis and monitored the stability of existing RORβ (**Fig 3b**). CHX was administered at timepoint beginning 24 hours post-transfection. Addition of p300 increased RORβ protein abundance relative to cells transfected with RORβ alone, with timepoints 2 and 4 hours after CHX treatment showing significantly enhanced abundance of RORβ co-transfected with p300 relative to cells transfected with RORβ alone. To investigate the effect of p300 on RORβ activation of transcription, we decided to indirectly infer the regulatory process using an ROR response element (RORE) luciferase reporter system (**Fig 3c**). HEK 293T cells were transiently transfected with RORβ +/- p300 followed by 18h treatment with SIRT1 inhibitor, EX-527. Treatment with the sirtuin inhibitor, EX-527 had little effect on reporter activity in RORβ+p300 cells, which were similar to vehicle. In cells transfected with RORβ alone, EX-527 reduced luciferase activity to 56% that of untreated control. Comparing the untreated controls for the RORβ and RORβ+p300 samples shows that p300 increased reporter activity by 43%. The addition of p300 increased RORβ signal in immunoblots and increased RORβ activity in the reporter assay. One mechanism for this may be through p300 increasing RORβ stability. Combined, these observations suggest SIRT1-dependent deacetylation of p300 alters the conformation of p300 in complex with RORβ resulting in reduced turnover of the receptor.

RORβ is acetylated by p300 in the DBD and hinge, deacetylated by SIRT1, and ubiquitinated in the hinge and LBD

To identify the relationship between RORβ protein stability and acetylation by p300, we investigated acetylation sites on RORβ. HEK 293T cells were transiently transfected with HA-RORβ +/- p300 and with or without SIRT1. The immunoprecipitated HA-RORβ was subjected to mass spectrometric analysis. Seven acetylated lysines were identified on RORβ, five of which were in the DBD, one in the C-terminal extension of the DBD, and one in hinge region (**Fig. 4a**). No acetylated lysines were detected in the LBD region. Sites K11, K69, K81 and K99 displayed some baseline acetylation, presumably by endogenous acetyltransferases; however, co-transfection with p300 significantly increased the abundance of acetylated peptides for residues K16, K31, K81, K99, and K176. RORβ site K176, located in the disordered hinge region, showed the greatest acetylation upon co-transfection with p300, which exhibited comparatively low endogenous acetylation. In the presence of SIRT1, acetylation at K176 was undetectable; however, RORβ co-transfected with p300 yielded a peptide with a distinct extracted ion chromatogram and robust fragmentation spectrum (**Fig. 4b, c**). To show the identified

acetylation sites in the context of DNA-binding, an AlphaFold 3.0 model of RORβ complexed with RORE DNA oligomer (5'-AGGTCA-3') was constructed (**Fig. 4d**). Using mass spectrometric analysis, we confirmed that the hinge region of RORβ undergoes p300-dependent acetylation and is subsequently deacetylated by SIRT1.

One potential explanation for the stabilizing effect of p300 on RORβ is through p300 mediated acetylation modulating ubiquitination of the receptor. Therefore, ubiquitinated sites of RORβ were also investigated, both in the presence and absence of the proteasome inhibitor MG-132. Trypsin digest of ubiquitinated proteins leaves a diglycine "GG" modification on the ubiquitin-modified lysines, readily detectable by mass spectrometry. Five ubiquitin sites were identified (**Fig. 4a**): K176 and K179 in hinge, K398 and K408 in the LBD, and the C-terminal residue K459. Ubiquitinated sites were only identified in RORβ co-transfected with p300 and SIRT1. Three of these ubiquitination sites: K176, K179, and K459 were only detected in cells treated with MG-132. Interestingly, an RORβ mutant mimicking constitutive acetylation at K176Q did not show ubiquitin GG modifications (**Fig. S3**).

SIRT1 coordinates with p300 to enhance the abundance and transcriptional activity of RORβ

SIRT1 is a nicotinamide adenosine dinucleotide (NAD) dependent class 3 histone deacetylase that removes acetyl groups from lysines for numerous proteins including nuclear receptors (*35*), and has been shown to act on RORγt (*32*), which shares 48% sequence identity with RORβ (**Fig. S4**). Additionally, because the SIRT1 inhibitor EX-527 showed reduction of RORβ activity in RORE reporter assay, we hypothesized that SIRT1 is deacetylating RORβ. Western blots of cell lysates transiently transfected with RORβ +/- p300 and SIRT1 showed co-transfection of RORβ, p300, and SIRT1 led to five-fold increase in levels of RORβ compared to cells transfected with RORβ alone, and a 2-fold increase relative to cells transfected with RORβ and p300 (**Fig. 5a**).

To further assess the effect of acetylation on RORβ transcriptional activity, mutants were designed at residues K176 and K179. Because K176 showed the greatest increase in acetylation upon treatment with p300, as well as being removed by SIRT1, we selected K176 as a mutation site. A K176Q mutant was designed as a constitutively acetylated mimic, and K176R is a mimic of the non-acetylated lysine. Additionally, analysis of SUMO motifs showed a strong consensus site containing residue K179 (**Fig. S5**) and the RIME IP-MS experiment identified E3

SUMO ligase RANBP2 (**Fig. 3c**) as a potential interactor of RORβ, so a K179R mutant was prepared that was not susceptible to SUMOylation at K179. By immunoblot, transiently transfected mutants showed similar protein abundance levels as WT (**Fig. S6**). In a RORE-luciferase reporter assay, K176Q did not show significant differences relative to WT. Mutant K176Q showed elevated transcriptional activity (**Fig 5b**). For each mutant, SIRT1 inhibitor EX-527 resulted in decreased activity relative to DMSO (**Fig. 5c**). RORβ luciferase activity was highest in cells transfected RORβ and p300, and the addition of SIRT1 did not have a significant effect (**Fig. 5d**).

A potential explanation for the effect of SIRT1 on RORβ levels is an indirect effect where SIRT1 increases the levels of p300 which in turn stabilize RORβ. In agreement with this hypothesis, quantitative comparison of protein abundances in samples co-immunoprecipitated by RORβ show that p300 levels are significantly increased in cell transfected with RORβ+p300+SIRT1 relative to cells transfected with RORβ+p300 (**Fig 5e**). This is corroborated by an AlphaFold 3.0 model of the ternary complex of p300, SIRT1, and RORβ which shows SIRT1 making extensive contacts with p300 (**Fig. S7**). However, in an analogous experiment performed with K176Q, p300 did not change significantly.

Further effects of SIRT1 were observed by changes in abundance of SUMO2 as well as the critical SUMOylation enzymes UBE21 and SENP1 co-immunoprecipitated with RORβ. These proteins were abundant in samples transfected with RORβ and p300, but significantly reduced when RORβ was immunoprecipitated from cells transfected with RORβ, p300, and SIRT1. This effect was recapitulated in corresponding experiments with the K176Q mutant, implying acetylation at K176 is not involved in the effect of SIRT1 on SUMO proteins interacting with RORβ.

Acetylation of RORβ by p300 does not reduce DNA binding by RORβ

The presence of p300 results in increased abundance of RORβ and upregulation of its transcriptional activity, and although acetylation was detected in the RORβ DBD, the increased transcriptional activity of RORβ by p300 implies that acetylation does not inhibit DNA binding by RORβ. In order to test this, p300 and RORβ were isolated in an in vitro system, and recombinant full length RORβ was incubated with full length recombinant p300 and the acetyltransferase substrate acetyl coenzyme A (Ac CoA). Immunoblot staining for acetyl lysine following incubation of RORβ with p300 and Ac CoA showed increased acetylation of RORβ

(**Fig. 6a**). The acetylated RORβ was subjected to an electrophoretic mobility shift assay (EMSA) in the presence of a 40-bp DNA oligo containing a single RORE sequence. In the EMSA assay, acetylation by p300 did not show either a reduction in the signal of RORβ bound DNA, or an increase in the signal of unbound DNA relative to the controls, indicating acetylation of RORβ did not affect its DNA binding (**Fig. 6b**). Since p300 acetylation of RORβ does not appear to inhibit DNA binding, it might be expected that DNA binding by RORβ would not influence acetylation of RORβ by p300, as access to acetylation sites would not be hindered by DNA binding. Acetylation of RORβ by p300 in the presence and absence of the DNA oligomer did not show a significant effect on the extent of acetylation by p300 (**Fig. 6c, d**).

DISCUSSION

RORβ is primarily expressed in retinal cells and the brain where it is enriched in astrocytes although the receptor is expressed in many other tissues. It has been shown that abnormally low expression of RORβ can lead to blindness, osteoarthritis, cancer, or neurological disorders. Despite this, little is known about its regulatory mechanisms. Here, using IP-MS, MSMS and structural proteomics, we were able to identify the acetylated and ubiquitinated lysine residues of RORβ, as well as the proteins that bind to and modify RORβ. *EP300*, a histone acetyl transferase (HAT) that regulates gene transcription mediated via chromatin remodeling, was enriched by RORβ immunoprecipitation. Addition of p300 increased the transcriptional activity of RORβ and enhanced lysine acetylation within the DBD and hinge domains.

Postulating that deacetylation influences RORβ's transcriptional activity, we investigated the effects of SIRT1, a previously identified deacetylase for the subfamily member RORγ, on RORβ's transcriptional activation. Our findings unveil an intricate interplay between SIRT1, p300, and RORβ, revealing a complex regulatory mechanism that influences protein stability, transcriptional activity, and post-translational modifications. The deacetylation of RORβ by SIRT1 not only enhances its transcriptional activity but also increases the stability of both RORβ and p300 when in complex. Notably, p300-mediated acetylation of the hinge region at K176 of RORβ appears to protect the receptor from ubiquitin-mediated degradation. Our crosslinking data suggests an intimate spatial proximity between the p300 "RING" domain and both the DBD and LBD of RORβ. This proximity may be crucial for modulating histone acetyltransferase activity to facilitate receptor transactivation activity.

To further elucidate these mechanisms, we plan to investigate the effects of SIRT1 on p300 stability using site-directed mutagenesis of various lysine residues identified to interact with RORβ in the cross-linking studies. Additionally, there is evidence that RORβ is SUMOylated or involved in SUMOylation pathways and that this is affected by SIRT1. A next step would be a search for RORβ SUMOylation sites. While detecting ubiquitination sites is relatively straightforward, detection of SUMOylation sites requires specialized mass spectrometry approaches. These studies will provide valuable insights into the complex regulatory network governing RORβ function. Understanding these intricate interactions and their effects on protein stability, transcriptional activity, and post-translational modifications should pave a path for novel therapeutic approaches in treating diseases associated with RORβ deficiency or loss of function. By targeting the SIRT1-p300-RORβ axis, we may be able to develop more effective and precise interventions for conditions such as retinal degeneration, osteoarthritis, RORβ associated cancers and certain neurological disorders.

MATERIALS and METHODS

Cell line and transfection

For rapid immunoprecipitation mass spectrometry of endogenous proteins (RIME) experiments TC28a2 human chondrocytes (Sigma) were transfected with human His-HA-RORβ (or pCMV6 base vector for control samples) using Xtreme Gene HP DNA reagent (Roche) at 70 to 80% confluency at a ratio of 3:1 reagent to DNA. Cells were harvested 24 hours after transfection. HEK 293T (ATCC) cells were used for Western blots, RORE-luciferase reporter assays, and mass spectrometry of analysis of acetylation and ubiquitination. HEK 293T cells were transfected at a 1:2:3 ratio of His-HA-RORβ (pCMV6), myc-p300 (pCMVβ), SIRT1 (pECE). Cells were transfected with polyethylenimine (PEI) reagent at 70 to 80% confluency at a ratio of 3:1 PEI to DNA. Total transfected DNA was held constant by adding empty vector. pCMVβ-p300-myc was a gift from Tso-Pang Yao (Addgene plasmid #30489). Mycoplasma tests were performed every 6 months. Both TC28a2 and HEK 293T cells were maintained in Dulbecco's modified Eagle's medium (DMEM) supplemented with 10% fetal bovine serum (FBS) with antibiotics (penicillin/streptomycin; Invitrogen).

Reporter assay

HEK 293T cells were transfected with 5X-RORE-luciferase (pGL4.14), His-HA-RORβ (pCMV6) and myc-p300 (pCMVβ) at a ratio of 1:1:2. For experiments with SIRT1, a ratio of 1:1:2:3 was used for 5X-RORE-luciferase (pGL4.14), His-HA-RORβ (pCMV6), myc-p300 (pCMVβ) and SIRT1 (pECE). 24 hours after bulk transfection, cells were transferred to a 384 well plate (to each well was added 20 µL of 0.5 x 10^6 cells/mL). After 3 hours at 37 °C, compounds (or DMSO) were introduced (in 20 µL media) and incubated for 18 hours. Following this, cells were lysed with BriteLite reagent (Perkin Elmer) for 3 minutes at RT, and luciferase activity was measured. Results were analyzed using GraphPad Prism software. A similar approach was used for reporter assays with various RORβ mutants.

RIME IP-MS

The RIME experiment RORβ was done using an adapted protocol for formaldehyde crosslinking of chromatin complexes followed by immunoprecipitation (*33*). Approximately 1.5 x 10^7 cells were used per bioreplicate (n=3). 24 hours after transfection, cells were washed with PBS and media was replaced with freshly prepared room temperature DMEM (serum free) containing 1% formaldehyde (Thermo Scientific, 28908). After 8 minutes at room temperature, the reaction was quenched by adding glycine (1.0 M, pH 7.5) to a final concentration of 100 mM. Cells were washed twice with cold PBS, harvested, and treated with lysis buffer to remove cytoplasmic proteins (50 mM HEPES-KOH, (pH 7.5), 140 mM NaCl, 1 mM EDTA, 10% (vol/vol) glycerol, 0.5% (vol/vol) NP-40/Igepal CA-630 and 0.25% (vol/vol) Triton X-100 with HALT protease inhibitor (Thermo)), nuclei were pelleted by centrifugation and treated with lysis buffer 2 (10 mM Tris-HCL (pH 8.0), 200 mM NaCl, 1 mM EDTA and 0.5 mM EGTA, with HALT protease inhibitor). After centrifugation, pellet was resuspended in lysis buffer 3 (10 mM Tris-HCl (pH 8.0), 100 mM NaCl, 1 mM EDTA, 0.5 mM EGTA, 0.1% (wt/vol) sodium deoxycholate and 0.5% (vol/vol) N-laurylsarcosine) and DNA was fragmented with sonication (Corvaris). Triton X-100 was added to 1% and samples were centrifuged (20,000 x *g*, 10 min, 4 °C). Supernatant was mixed with anti-HA magnetic beads (Pierce) and incubated at 4 °C overnight with rotation. Beads were washed nine times (50 mM HEPES (pH 7.6), 1 mM EDTA, 0.7% (wt/vol) sodium deoxycholate, 1% (vol/vol) NP-40 and 0.5M LiCl) followed by two washes with 100 mM ammonium bicarbonate. Beads were digested with trypsin overnight at 37 °C (0.5 µg trypsin, 100 mM ammonium bicarbonate). Following trypsin digestion, peptides were desalted with ziptip (Millipore, ZTC18S09) following the manufacturer's protocol.

Expression and purification of recombinant RORβ

Strep-SMT3-His-RORβ(2-459, human) was codon optimized for *E. Coli* expression and inserted into a pET-28a(+) plasmid (Genscript). After transformation (Agilent, BL21 CodonPlus (DE3)-RIL, 230245) cells were grown on agar supplemented with kanamycin and single colonies were used to prepare overnight culture in terrific broth with kanamycin. Overnight culture (0.5 mL) was added to 250 mL terrific broth media (with kanamycin) containing 30 µM $ZnCl_2$, grown at 37 °C to an OD_{600} of 0.6-0.8, and the temperature was reduced to 16 °C. IPTG was added to 250 µM and the media was shaken for an additional 15 h. Cells were harvested (4,000 x *g*, 20 min, 4 °C) and lysed (50 mM HEPES, pH 8.0, 500 mM NaCl, 10% glycerol, 1 mM DTT, 1 mM $MgCl_2$, with 0.25 mg/mL lysozyme, 400 units benzonase, with HALT protease inhibitor and 1 mM PMSF, 30 mL total volume, 30 minutes on ice) followed by 2 minutes sonication at 70% amplitude. Sample was clarified (20,000 x *g*, 15 minutes, 4 °C) and flowed over 1.1 mL volume streptactin column (Streptactin XT superflow, Zymo Research, ZRE160702). Flow through was collected and added to the column a second time, then the column was washed with 5 column volumes of wash buffer (50 mM HEPES, pH 8.0, 500 mM NaCl, 10% glycerol). SUMO protease (Ulp1) was added (1.0 µg in 1.0 mL 50 mM HEPES, pH 8.0, 500 mM NaCl, 10% glycerol, 5 mM DTT) and incubated 1 h at RT. Sample was eluted in 3.0 mL (50 mM HEPES, pH 8.0, 500 mM NaCl, 10% glycerol, 5 mM DTT) and stored in 50% glycerol at -20 °C.

Expression and purification of recombinant p300

Human p300 as full-length open reading frame DNA was synthesized with optimal codon usage for insect cells with an in-frame Strep II tag (WSHPQFEK/G) and a glycine spacer at the amino-terminus and inserted into pFastBac1 transfer vector (Epoch Life Sciences, Houston, TX). Recombinant bacmid was generated and expanded in Spodoptera frugiperda (Sf9) cell cultures and viral titer was determined by plaque assays as previously described.[38, 39] Multiple 500 mL cultures of SF9 cells were infected with recombinant virus at an MOI of 2.0 and incubated for 48 hour at 27°C in oxygenated spinner vessels. Cells were collected and centrifuged 1500x g for 10min and pellets were washed once PBS by resuspension and centrifugation. Cell pellets were flash frozen and stored at -80°C. Cells (from 2x 500ml cultures) were resuspended in 50 mL of lysis buffer (50 mM Na_2HPO_4, pH 8.0, 500 mM NaCl, 5% Glycerol, 1 M Urea, 1 mM EDTA, 1 mM 2ME), supplemented with protease inhibitor tablets (leupetin, aprotinin, bacitracin, and PMSF) and submitted to Teflon-glass homogenization for 8 strokes at 1.5 speed in the cold room (4°C). The homogenate was treated with 1.2 units/mL of benzonase nuclease or 1 hour at 4°C then passed 3 times through an 18G needle followed by a 25G needle. The lysate was centrifuged twice for 1 hour at 50,00 xg and the resulting supernatant was filtered using 0.2 µm

disposable filters. Purification was performed on AKTA Pure™ 25 at 4 °C while monitoring conductivity and UV. A 1 mL StrepTrap XT prepacked Hi-Trap chromatography column (Cytiva) was equilibrated with lysis buffer for 10 column volumes (CV), and after loading the cleared cell lysate, the column was washed for 30 CV with equilibration buffer and then eluted with equilibration buffer containing 40 mM biotin. Eluted fractions (1 mL) were collected and analyzed by Coomassie Blue-stained 4-15% gradient SDS-PAGE gel. Fractions containing p300 were pooled and concentrated to 1-2 mL by an Amicon ultracentrifugal device with a 10,000 MW cutoff (A280<4.0). Protein was further purified by a preparative size exclusion chromatography (SEC) column (HiLoad 16/600 Superdex 200pg), degassed and equilibrated in SEC buffer (20 mM Hepes, pH 7.5, 200 mM NaCl, 5% Glycerol, 1 M Urea and 1 mM TCEP). Elution fractions (1 mL) were collected and analyzed by Coomassie Blue-stained 4-15% gradient SDS-PAGE gels and peak fractions were concentrated as above. Concentration of p300 was by determined by Nanodrop absorbance at 280/260 nm, calculation of extinction coefficient, and by comparison of purified bands on Coomassie Blue-stained 4-15% SDS-PAGE gel with a standard curve of know amounts of unstained protein markers. Aliquots (50-100 µL) of p300 were snap frozen in liquid nitrogen and stored at -80°C for up to 3-4 months and samples were used only once after thawing.

RORβ-dependent p300 pulldown

For p300 pulldown with recombinant His-RORβ we followed an adapted protocol (*36*). RORβ (32 µg, 40 µL of 0.8 mg/mL, or 40 µL RORβ buffer for control) was added to 0.5 mL 1% bovine serum albumin (BSA) in IP/lysis buffer (Pierce, 87788) and incubated with MagneHis beads (Promega, 32 µL suspension, 5 minutes RT, 10 minutes, 4 °C). Beads were washed once (500 µL, IP/lysis buffer) and a second time (500 µL IP/lysis buffer with 1% BSA) and blocked (100 µL IP/lysis buffer with 1% BSA, 4 °C). Cell lysate was prepared from approximately 2 x 10^7 HEK 293T cells transiently transfected with myc-p300 (2 mL Pierce IP/lysis buffer), sonicated (2 x 5 s, amplitude 8), centrifuged (20,000 x *g*, 10 min, 4 °C), and incubated with Magnetic-His beads (900 µL total lysate volume, 30 minutes at RT). Beads were washed four times (300 µL IP/lysis buffer with 10 mM imidazole) then eluted (50 µL 300 mM imidazole, PBS, pH 8.0 with 6X SDS-PAGE gel loading buffer (non-reducing), 95 °C, 5 min.). Eluate was removed from beads, DTT was added to 40 mM, sample was heated (95 °C, 3 min.). Input (i.e., lysate) was heated at 95 °C 5 minutes (with 6X SDS-PAGE loading buffer with 40 mM DTT). SDS-PAGE was performed with 20 µL of lysate or eluate. After Western blot transfer for high molecular weight proteins (BioRad Trans-turbo, 13 Amps, 25 Volts, 10 min) membrane was immunoblotted for p300 (BD

Pharmingan, 554215) and myc (Cell Signaling, 9B11). On a separate membrane RORβ was immunoblotted for (Novus, NBP2-45610).

CHX protein stability

HEK 293T cells were transfected and after 42 h, cycloheximide (CHX) was added at 10 µM at intervals of 4, 2, 1, and 0 h (0 h treated with DMSO only). Cells were washed with PBS, harvested and lysed (250 mM NaCl, 0.1% NP-40, 20 mM NaH2PO4, pH 7.5, 5 mM EDTA, 30 mM sodium pyrophosphate, 10 mM NaF with HALT protease inhibitor (Thermo Fisher Scientific)), and centrifuged (16,000 x *g*, 10 min, 4 °C). Protein concentration was measured with Pierce 660 assay (Thermo Scientific), and 10 µg protein was loaded per well for SDS-PAGE. Following transfer, membranes were immunoblotted (RORβ (Novus, NBP2-45610), β-actin (Cell Signaling, 13E5) 1000:1 ratio, overnight, 4 °C). Membranes were washed (3 x 5 min, TBST), treated with secondary antibodies (Li-COR, anti-rabbit 926-32211, anti-mouse 926-68070, 15,000:1, 1 h, RT) and imaged (Li-Cor). Fluorescence signal was quantified with Empiria Studio software (Version 2.3.0.154) and data was analyzed in GraphPad Prism (Version 6.01).

***In cellulo* RORβ acetylation and ubiquitination analysis**

RORβ acetylation was analyzed by adapting a prior method (*32*) HEK 293T cells were transfected and after 30 min, trichostatin A (TSA) was added to a concentration of 400 nM. After 24 h, cells were washed 1 x with ice cold PBS and harvested (approximately 1.5 x 10^7 cells). Cells were lysed (250 mM NaCl, 0.1% NP-40, 20 mM NaH2PO4, pH 7.5, 5 mM EDTA, 30 mM sodium pyrophosphate, 10 mM NaF with HALT protease inhibitor (Thermo Fisher Scientific), 400 nM TSA, 5 mM NAM) for 20 min on ice. Sample was clarified and incubated with 100 µL anti-HA magnetic beads (Pierce, 45 min, RT), washed (5 x, 1 mL IP/lysis buffer (Pierce) supplemented with additional 100 mM NaCl). Sample was eluted (95 °C, 5 min, 25 µL non-reducing lane marker (Thermo Scientific) and loaded onto SDS-PAGE gel. Bands for RORβ were excised from the gel, washed (200 µL 1:1 acetonitrile/50 mM ammonium bicarbonate, 20 min, 1000 rpm, followed by 50 mM ammonium bicarbonate, 20 min, 1000 rpm). Band was dehydrated (100 µL acetonitrile, 5 min speedvac), then reduced (200 µL, 25 mM DTT, 30 min, 56 °C), alkylated (200 µL, 55 mM iodoacetamide, in dark, 30 min), washed twice (400 µL water), dehydrated, and digested with trypsin (0.1 µg, 200 uL 50 mM ammonium bicarbonate, 18h). Peptides were extracted twice (1:1 acetonitrile / 0.1% TFA, 20 min), dried, and desalted with ziptips (Millipore, ZTC18S09).

To search for ubiquitin modifications a similar immunoprecipitation strategy was employed. Proteins were digested on-bead with a combination of trypsin and chymotrypsin. Four hours prior to harvesting cells, MG-132 (or DMSO) were added to cell media to a concentration of 20 µM. A low concentration of iodoacetamide (1 mM) was included during cell lysis and immunoprecipitation at 4 °C to inhibit deubiquitinases, but samples were not reduced and alkylated to avoid high concentrations of iodoacetamide which could acylate lysine residues (*37*). Data was analyzed in Proteome Discoverer and manually validated in Skyline. The area under curve of the extracted ion chromatogram was derived from Skyline and normalized based on total number of peptide spectral matches for RORβ found in each sample.

Liquid chromatography and tandem mass spectrometry

Samples were injected (duplicate or triplicate injections) onto an UltiMate 3000 UHP liquid chromatography system (Dionex, ThermoFisher). Peptides were trapped using a µPAC C18 trapping column (PharmaFluidics) using a load pump operating at 20 µL/min. Peptides were separated on a 200 cm µPAC C18 column (PharmaFluidics) using a linear gradient (1% Solvent B for 4 min, 1–30% Solvent B from 4 to 70 min, 30–55% Solvent B from 70 to 90 min, 55–97% Solvent B from 90 to 112 min, and isocratic at 97% Solvent B from 112 to 120 min) at a flow rate of 800 nL/min. Gradient Solvent A contained 0.1% formic acid, and Solvent B contained 80% acetonitrile and 0.1% formic acid. Liquid chromatography eluate was interfaced to an Orbitrap Fusion Lumos Tribrid mass spectrometer (ThermoFisher) with a Nanospray Flex ion source (ThermoFisher). The source voltage was set to 2.5 kV, and the S-Lens RF level was set to 30%. Full scans were recorded from m/z 150 to 1500 at a resolution of 60 000 in the Orbitrap mass analyzer. The AGC target value was set to 4×10^5, and the maximum injection time was set to 50 ms in the Orbitrap. For acetylation analysis, MS2 scans were recorded at a resolution of 15,000 in the Orbitrap mass analyzer. The AGC target was set to 5×10^4, with a maximum injection time of 200 ms, and an isolation width of 1.6 m/z. For RIME analyses, MS2 was performed in the iontrap, with an isolation width of 1.2 m/z using a turbo scan rate and dynamic maximum inject time. For ubiquitination analyses, FAIMS was included with compensation voltages of –45 and –60 V. Cross-links were identified using a previously described MS2-MS3 method with slight modifications (*38*). Full scans were recorded from m/z 150 to 1500 at a resolution of 60 000 in the Orbitrap mass analyzer. The AGC target value was set to 4×10^5, and the maximum injection time was set to 50 ms in the Orbitrap. MS2 scans were recorded at a resolution of 30 000 in the Orbitrap mass analyzer. Only precursors with a charge state between 4 and 8 were selected for MS2 scans. The AGC target was set to 5×10^4, a maximum

injection time of 150 ms, and an isolation width of 1.6 m/z. The CID fragmentation energy was set to 25%. The two most abundant reporter doublets from the MS2 scans with a charge state of 2–6, a 31.9721 Da mass difference, and a mass tolerance of ±10 ppm were selected for MS3. The MS3 scans were recorded in the ion trap in rapid mode using HCD fragmentation with 35% collision energy.

Cross-linking Mass Spectrometry (XL-MS)

Crosslinking of His-RORβ with p300 (His-SUMO-p300 residues 1040-1850, human) was performed with 3 µM of each protein with DSSO crosslinker (1.5 mM DSSO, 1 h, RT. buffer: HEPES 25 mM, pH 7.7, 150 mM NaCl, 1 mM TCEP, 5% glycerol). Crosslinking reactions were performed in triplicate for both DSSO and DMSO controls. Putative crosslinkers were identified in proteome discoverer with the XlinkX algorithm workflow and imported into Skyline for manual inspection and validation.

RORβ *in vitro* acetylation by p300 and EMSA

Full length recombinant human RORβ was incubated with full length recombinant human p300, with 1 mM acetyl CoA (Sigma) at a 20:1 w/w ratio of RORβ to p300 (HEPES 50 mM, 10 mM sodium butyrate, 7.5% glycerol, 1 mM DTT, HALT protease inhibitor, pH 8.0; 1 h at 30 °C). Reactions were carried out with RORβ at concentrations of 4.0 µM and 2.0 µM. For DNA binding EMSA assay, the above acetylation reactions were incubated with DNA (0.25 µM) in ratios of 8:1 and 4:1 RORβ to DNA (sequence 5'-ATTTAAAGTGGGTCAGAAAATTTTCTGACCCACTTTAAAT-3') respectively (HEPES 25 mM, 5 mM sodium butyrate, 3.75% glycerol, 0.5 mM DTT, 200 mM NaCl, 10 mM MgCl2, HALT protease inhibitor, pH 8.0; 20 min, RT) and assayed on an 8% nondenaturing polyacrylamide gel (200 V, 40 min, 4 °C).

Mutant RORβ Generation

RORβ mutants K176R, K176Q, and K179R were generated from human His-HA-RORβ in pCMV6 base vector with using the primers K176R forward (5'-GACTGGAATCCGCCAGATAAAGCAAGAAC-3') K176R reverse (5'-ATGTCAAGTCCTGACTG-3'), K176Q forward (5'-GACTGGAATCCAGCAGATAAAGCAAG-3') and K176Q reverse (5'-ATGTCAAGTCCTGACTG-3'), K179R forward (5'-CAAACAGATACGCCAAGAACCTATCT ATGACC-3') and K179R reverse (5'- ATTCCAGTCATGTCAAGTC-3') using NEB Q5 site-directed mutagenesis kit (#E0552).

Data deposition

All MS data has been submitted to the ProteomeXchange Consortium via the PRIDE partner repository with the dataset identifier, PXD058187. Reviewers may access the dataset using token HpqGN8m2OKfN. Alternatively, reviewers can access the dataset with username: reviewer_pxd058187@ebi.ac.uk with password FvTW3yAZeseq.

Acknowledgments:

The authors acknowledge the expert assistance of the Recombinant Protein Production and Characterization Core (RPPCC) for expression of recombinant proteins in the baculovirus insect cell system. The RPPCC at BCM are supported by the NCI Cancer Center Support Grant (P30 CA125123) of the Dan L Duncan Comprehensive Cancer Center. The authors thank Drs. Dmitry Lyumkis and Timothy Strutzenberg for providing the truncated p300 core protein.

Figures

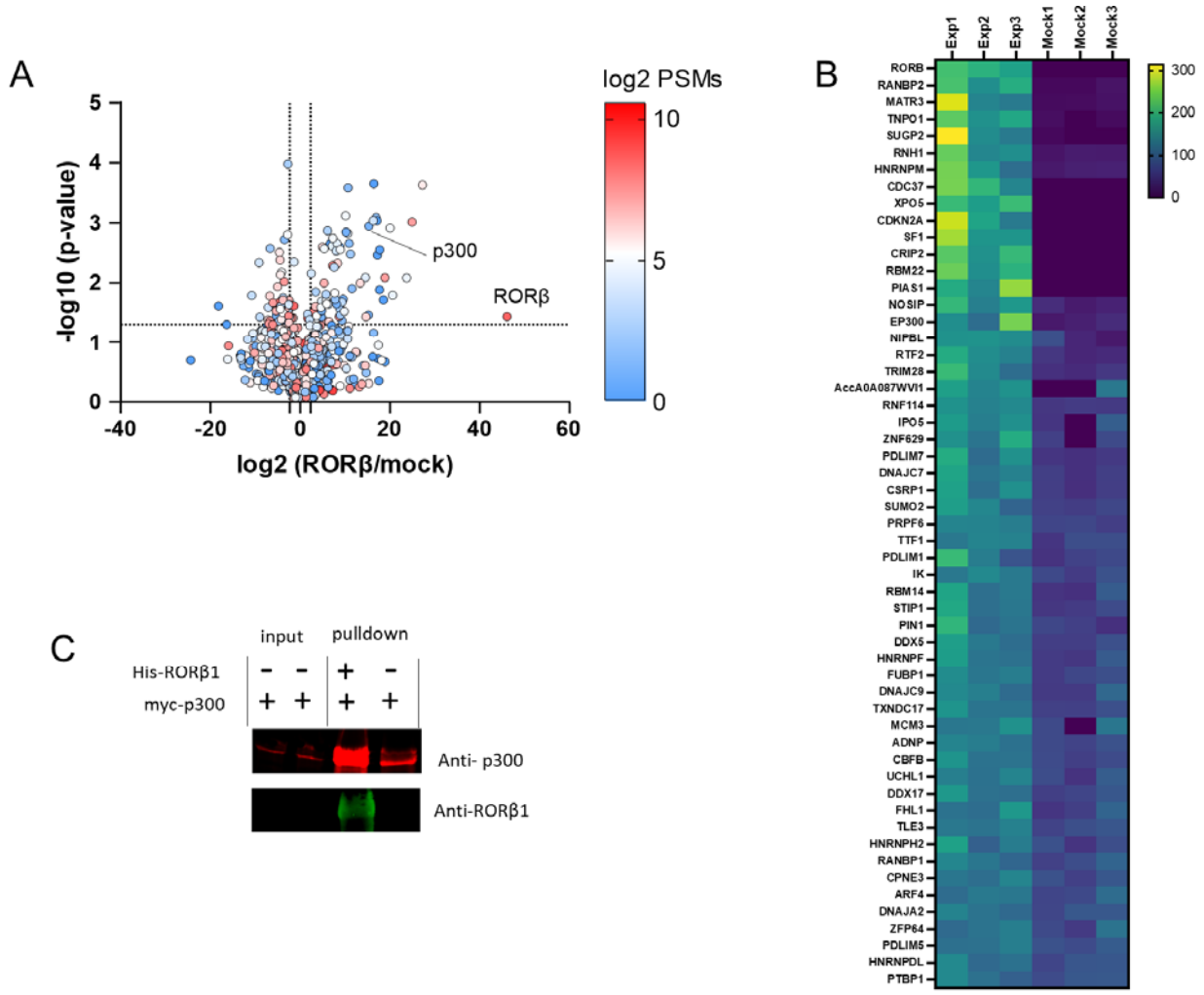

Figure 1. p300 is a direct interactor of RORβ. A) TC28a2 chondrocytes were transiently transfected with either HA-RORβ or mock (base vector), followed by formaldehyde crosslinking in live cells, immunoprecipitation with HA antibody, and mass spectrometry analysis. Volcano plot shows p-value vs enrichment ratio (ratio is protein abundance in HA-RORβ transfected cell lysate vs mock-transfected cell lysate, both immunoprecipitated with anti-HA beads). Horizontal lines represent 5-fold ratios, vertical lines show threshold for p-value of 0.05. Protein abundance as assessed by peptide spectral matches (PSMs) is represented by color gradient from blue to red. B) The abundance of 55 proteins with $p \leq 0.05$ from biological triplicate experiments, as shown in A, is represented in a heatmap. C) The interaction between p300 and RORB was validated by pulldown with recombinant RORβ. HEK 293T cells were transfected with myc-p300

and lysate was incubated with Ni beads +/- His-RORβ. Eluate from beads and input cell lysate was immunoblotted for myc-p300 or RORβ.

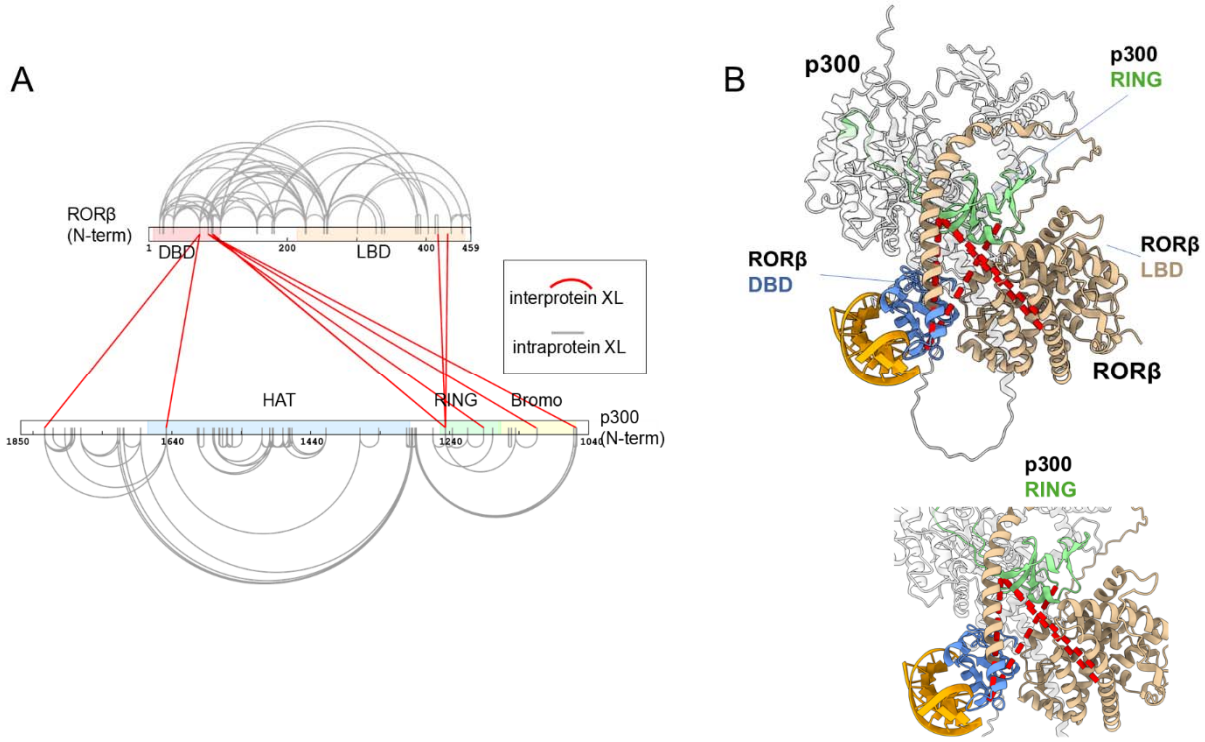

Figure 2. RORβ interacts with "RING" domain of p300. A) Crosslinking was performed with full length recombinant RORβ and a truncated p300 'core' comprising bromo, RING, and HAT domains (p300 core corresponds to residues 1040-1850). Crosslinking reactions were performed *in vitro* with both RORβ and p300 at a concentration of 3 μM, using the lysine-reactive crosslinker disuccinimidyl sulfoxide (DSSO). A) Eight high-confidence interprotein crosslinks were identified with six of these bridging p300 and the RORβ hinge/DNA-binding domain. B) Lysines identified in interprotein crosslinks from p300 RING domain to RORβ are shown (red) mapped to AlphaFold 3 structure of the RORβ:p300 complex with docked RORE DNA. The p300 ring domain is shown in light green and the inset shows a zoom on the RING domain.

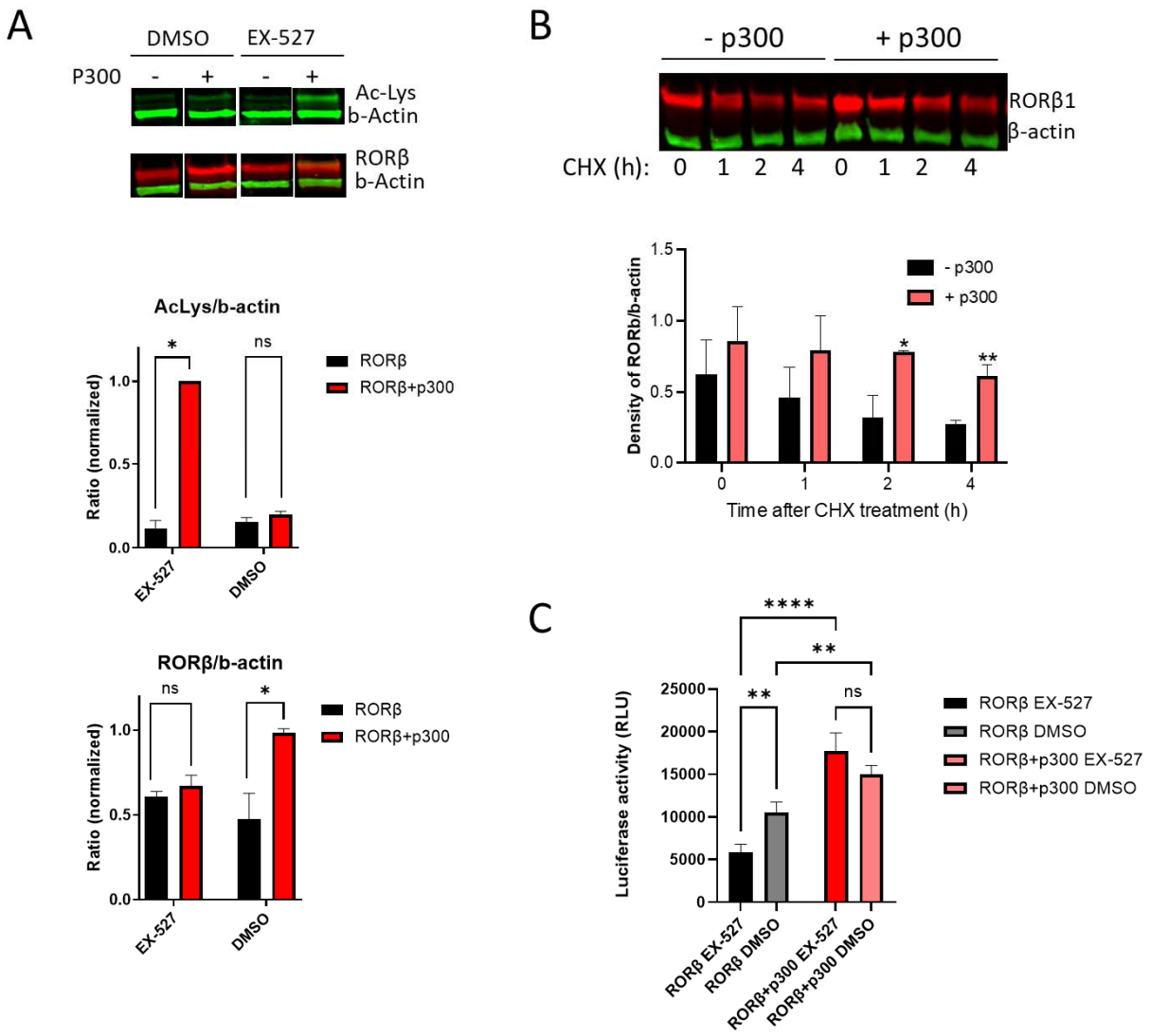

Figure 3. Effect of acetylation on RORβ protein stability and transcriptional activity. A) RORβ± p300 lysates blotted for RORβ and acetyl lysine. [EX-527 is a SIRT inhibitor, used at a concentration of 50 μM)]. b-actin was used for loading control. RORβ and acetyl lysine quantification, normalized with b-Actin. B) Effect of p300 on stability of RORβ protein. Following transfection, cycloheximide (CHX) was added at 10 μM and cells were harvested at the indicated time points after CHX addition. C) Transcriptional activity of RORβ. HEK 293T cells were transfected with RORβ, 5X RORE-luciferase and +/- p300 vectors, treated with 50 μM EX-527 for 18 h, after which luciferase activity was measured.

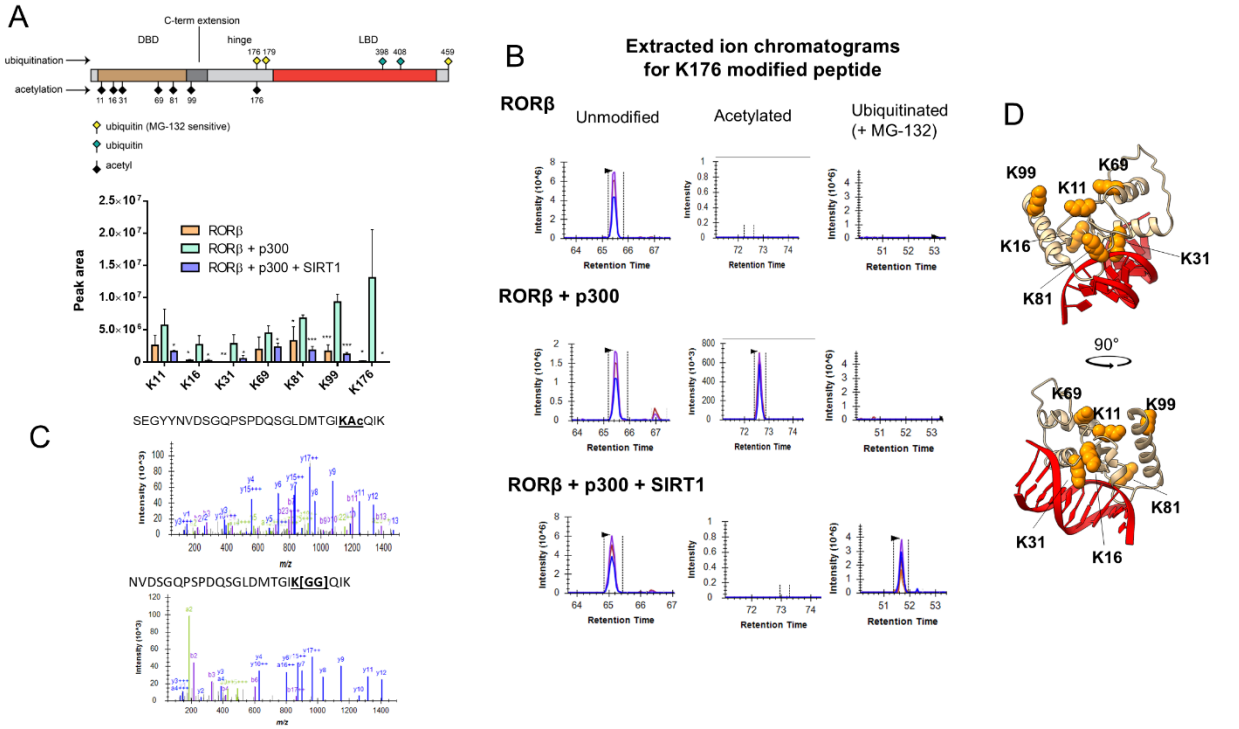

Figure 4. RORβ is acetylated by p300 and ubiquitinated following SIRT1 deacetylation. A) HA-RORβ was transfected into HEK 293T cells +/- p300 and SIRT1, followed by IP of RORβ and MS analysis and quantification. B) Extracted ion chromatograms (EIC) for peptide corresponding to K176 position, left panel is unmodified peptide, middle panels are acetylated, and right panel (+MG-132) is ubiquitinated at positions K176. C) Representative MS2 spectrum for acetylated and ubiquitinated peptide, annotated peaks are within 0.02 Da mass accuracy. SEGYYNVDSGQPSPDQSGLDMTGI**K[Ac]**QIK peptide is shown for acetylation, NVDSGQPSPDQSGLDMTGI**K[GG]**QIK peptide is shown for ubiquitination. D) Acetylated lysine sites of RORβ are shown as orange spheres on an AlphaFold 3 model of RORβ DBD in complex with RORE DNA (5'-AGGTCA-3').

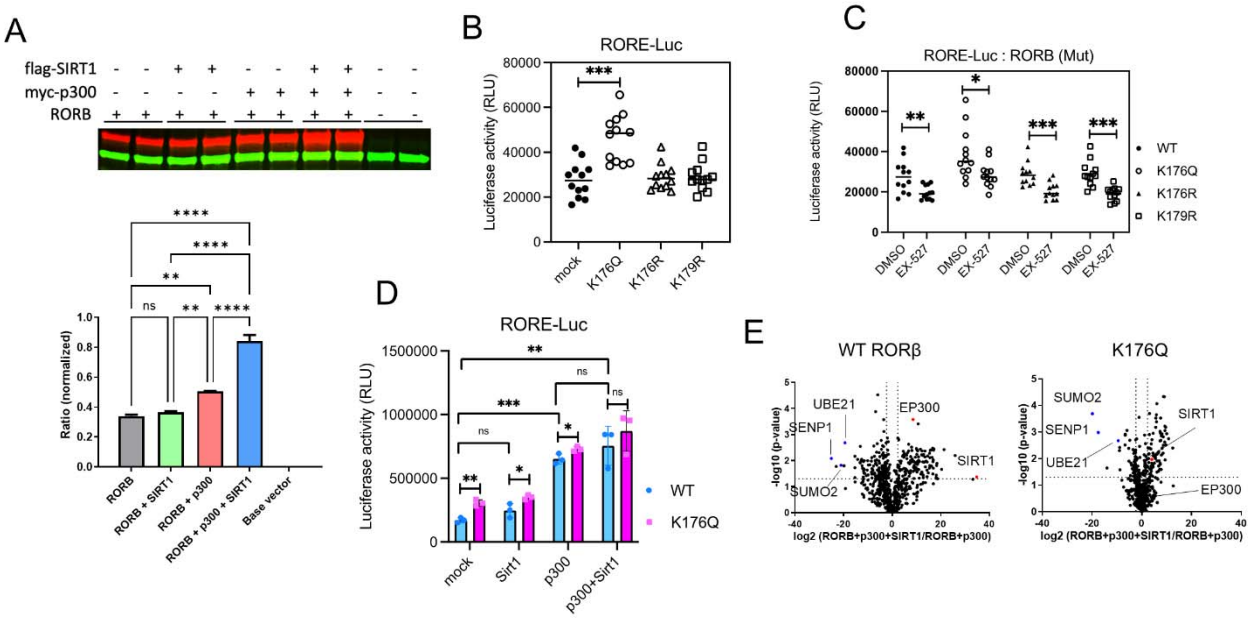

Figure 5. **SIRT1 increases RORβ abundance**. A) HEK 293T cells were transiently transfected with RORβ, p300 and SIRT1, followed by immunoblotting for RORβ and β-actin. Immunoblot fluorescence signal for RORβ was quantified and normalized to β-actin. B) RORE reporter assay comparing transcriptional activity for K176Q, K176R, and K179R mutants. The RORE reporter assay was performed with transiently transfected WT and mutant RORβ in HEK293T cells C) RORE reporter assay was performed with transiently transfected WT and mutant RORβ in HEK293T cells, each treated with 50 µM EX-527 or DMSO control. D) RORE-luciferase reporter assay was used to compare RORβ activity in cells transiently transfected with RORβ(WT), RORβ+p300, and RORB+p300+SIRT1 (blue bar) and K176Q (purple bar) mutants. E) Volcano plot showing changes in RORβ co-immunoprecipitated proteins in HEK 293T cells transfected with RORβ+p300+SIRT1 vs RORβ +p300 (for WT and K176Q RORβ). Equal amounts of p300 DNA were transfected in both samples. p300 shows significantly increased abundance in +SIRT1 sample for WT RORβ while showing no significant change in the K176Q sample.

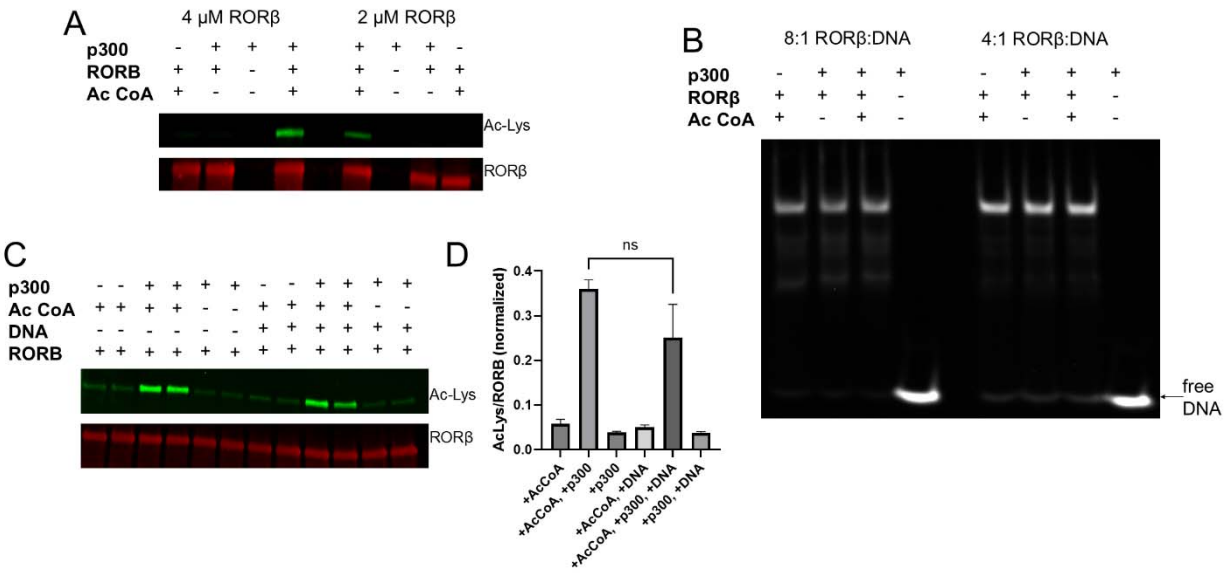

Figure 6. p300 acetylation of RORβ does not exhibit an effect on DNA binding in vitro. A) Full-length recombinant RORβ was incubated with full-length recombinant p300 in the presence of Ac CoA, followed by immunoblotting of the reaction mixtures for acetyl lysine and RORβ. Reactions were performed at two concentrations of RORβ. B) Following *in vitro* acetylation by p300, samples were incubated with a 40 bp DNA sequence (5'-ATTTAAAGTGGGTCAGAAAATTTTCTGACCCACTTTAAAT-3') containing the RORE motif and subjected to EMSA. Bound DNA is shown in the upper third of the gel and free DNA is at the bottom of the gel. C) RORβ was acetylated by p300 in the presence and absence of the 40 bp RORE sequence and immunoblotted for acetyl lysine and RORβ. D) The acetyl lysine signal from the blot shown in C was quantified and normalized to RORβ signal – no significant change in acetylation signal is observed upon addition of DNA.

Supplemental Figure 1. Gene ontology analysis for enriched proteins. 57 proteins were identified with significant ($p < 0.05$) fold-change (>5x) over negative control. This set of genes was analyzed for gene ontology (DOI: 10.1093/bioinformatics/bth456)

Supplemental Figure 2. A) Coomassie stained gel showing control and DSSO crosslinked samples for RORβ + p300 core. Red arrow highlights band that appears in DSSO treated sample at expected molecular weight of p300 complexed with RORβ. B) XL-MS with full length p300 and RORβ. Intraprotein crosslinks are shown in grey, interprotein crosslinks are red.

Supplemental Figure 3. Ubiquitin modifications are not detected on RORβ K176Q mutant. Skyline was used to calculate extracted ion chromatogram peak areas for GG modified peptides and a corresponding unmodified peptide. Note that for K459, the GG modification is MG-132 dependent and is therefore only observed in cells treated with the proteasome inhibitor.

Supplemental Figure 4. Sequence alignment of RORγt and RORβ.

Supplemental Figure 5. SUMO motif analysis of RORβ performed using Joined Advanced SUMOylation Site and Sim Analyzer (JASSA) webserver (DOI: 10.1093/bioinformatics/btv403).

Supplemental Figure 6. Anti-HA staining of HA-RORβ and its mutants HA-K176Q, HA-K176R, and HA-K179R.

Supplemental Figure 7. AlphaFold 3.0 model of p300, SIRT1, and RORβ.

Reference

1. M. R. Chang *et al.*, Unique Polypharmacology Nuclear Receptor Modulator Blocks Inflammatory Signaling Pathways. *ACS Chem Biol* **14**, 1051-1062 (2019).
2. M. R. Chang, B. Lyda, T. M. Kamenecka, P. R. Griffin, Pharmacologic repression of retinoic acid receptor-related orphan nuclear receptor gamma is therapeutic in the collagen-induced arthritis experimental model. *Arthritis Rheumatol* **66**, 579-588 (2014).
3. N. Kumar *et al.*, Identification of SR2211: a potent synthetic RORgamma-selective modulator. *ACS Chem Biol* **7**, 672-677 (2012).
4. B. C. Lo *et al.*, The orphan nuclear receptor RORalpha and group 3 innate lymphoid cells drive fibrosis in a mouse model of Crohn's disease. *Sci Immunol* **1**, eaaf8864 (2016).
5. L. A. Solt *et al.*, Suppression of TH17 differentiation and autoimmunity by a synthetic ROR ligand. *Nature* **472**, 491-494 (2011).
6. Y. Wang *et al.*, Identification of SR1078, a synthetic agonist for the orphan nuclear receptors RORalpha and RORgamma. *ACS Chem Biol* **5**, 1029-1034 (2010).
7. M. R. Chang, H. Rosen, P. R. Griffin, RORs in autoimmune disease. *Curr Top Microbiol Immunol* **378**, 171-182 (2014).
8. Y. Wang, N. Kumar, C. Crumbley, P. R. Griffin, T. P. Burris, A second class of nuclear receptors for oxysterols: Regulation of RORalpha and RORgamma activity by 24S-hydroxycholesterol (cerebrosterol). *Biochimica et biophysica acta* **1801**, 917-923 (2010).
9. A. M. Jetten, Recent advances in the mechanisms of action and physiological functions of the retinoid-related orphan receptors (RORs). *Curr Drug Targets Inflamm Allergy* **3**, 395-412 (2004).
10. F. R. Santori *et al.*, Identification of natural RORgamma ligands that regulate the development of lymphoid cells. *Cell Metab* **21**, 286-298 (2015).
11. C. Stehlin-Gaon *et al.*, All-trans retinoic acid is a ligand for the orphan nuclear receptor ROR beta. *Nat Struct Biol* **10**, 820-825 (2003).
12. D. R. Shalinsky *et al.*, A novel retinoic acid receptor-selective retinoid, ALRT1550, has potent antitumor activity against human oral squamous carcinoma xenografts in nude mice. *Cancer Res* **57**, 162-168 (1997).
13. D. Cai *et al.*, RORgamma is a targetable master regulator of cholesterol biosynthesis in a cancer subtype. *Nat Commun* **10**, 4621 (2019).
14. A. W. Ashton *et al.*, Acetylation of nuclear receptors in health and disease: an update. *Febs j*, (2022).
15. A. Haelens, T. Tanner, S. Denayer, L. Callewaert, F. Claessens, The hinge region regulates DNA binding, nuclear translocation, and transactivation of the androgen receptor. *Cancer Res* **67**, 4514-4523 (2007).
16. A. Warnmark, E. Treuter, A. P. Wright, J. A. Gustafsson, Activation functions 1 and 2 of nuclear receptors: molecular strategies for transcriptional activation. *Mol Endocrinol* **17**, 1901-1909 (2003).
17. E. Andre, K. Gawlas, M. Becker-Andre, A novel isoform of the orphan nuclear receptor RORbeta is specifically expressed in pineal gland and retina. *Gene* **216**, 277-283 (1998).
18. E. Andre *et al.*, Disruption of retinoid-related orphan receptor beta changes circadian behavior, causes retinal degeneration and leads to vacillans phenotype in mice. *EMBO J* **17**, 3867-3877 (1998).
19. M. M. Roforth, G. Liu, S. Khosla, D. G. Monroe, Examination of nuclear receptor expression in osteoblasts reveals Rorbeta as an important regulator of osteogenesis. *J Bone Miner Res* **27**, 891-901 (2012).

20. A. Serretti *et al.*, Genetic dissection of psychopathological symptoms: insomnia in mood disorders and CLOCK gene polymorphism. *Am J Med Genet B Neuropsychiatr Genet* **121B**, 35-38 (2003).
21. C. L. McGrath *et al.*, Evidence for genetic association of RORB with bipolar disorder. *BMC Psychiatry* **9**, 70 (2009).
22. H. A. Mansour *et al.*, Association study of 21 circadian genes with bipolar I disorder, schizoaffective disorder, and schizophrenia. *Bipolar Disord* **11**, 701-710 (2009).
23. C. A. McClung, Circadian genes, rhythms and the biology of mood disorders. *Pharmacol Ther* **114**, 222-232 (2007).
24. K. Leng *et al.*, Molecular characterization of selectively vulnerable neurons in Alzheimer's disease. *Nat Neurosci* **24**, 276-287 (2021).
25. L. Zhang *et al.*, Single-cell transcriptomic atlas of Alzheimer's disease middle temporal gyrus reveals region, cell type and sex specificity of gene expression with novel genetic risk for MERTK in female. *medRxiv*, (2023).
26. L. Jia *et al.*, Retinoid-related orphan nuclear receptor RORbeta is an early-acting factor in rod photoreceptor development. *Proc Natl Acad Sci U S A* **106**, 17534-17539 (2009).
27. M. M. Roforth, S. Khosla, D. G. Monroe, Identification of Rorbeta targets in cultured osteoblasts and in human bone. *Biochem Biophys Res Commun* **440**, 768-773 (2013).
28. R. Aquino-Martinez *et al.*, miR-219a-5p Regulates Rorbeta During Osteoblast Differentiation and in Age-related Bone Loss. *J Bone Miner Res* **34**, 135-144 (2019).
29. J. N. Farr *et al.*, Osteoprotection Through the Deletion of the Transcription Factor Rorbeta in Mice. *J Bone Miner Res* **33**, 720-731 (2018).
30. M. Y. Kim, E. M. Woo, Y. T. Chong, D. R. Homenko, W. L. Kraus, Acetylation of estrogen receptor alpha by p300 at lysines 266 and 268 enhances the deoxyribonucleic acid binding and transactivation activities of the receptor. *Mol Endocrinol* **20**, 1479-1493 (2006).
31. M. Fu, C. Wang, X. Zhang, R. G. Pestell, Acetylation of nuclear receptors in cellular growth and apoptosis. *Biochem Pharmacol* **68**, 1199-1208 (2004).
32. H. W. Lim *et al.*, SIRT1 deacetylates RORγt and enhances Th17 cell generation. *J Exp Med* **212**, 607-617 (2015).
33. H. Mohammed *et al.*, Rapid immunoprecipitation mass spectrometry of endogenous proteins (RIME) for analysis of chromatin complexes. *Nature Protocols* **11**, 316-326 (2016).
34. M. Delvecchio, J. Gaucher, C. Aguilar-Gurrieri, E. Ortega, D. Panne, Structure of the p300 catalytic core and implications for chromatin targeting and HAT regulation. *Nat Struct Mol Biol* **20**, 1040-1046 (2013).
35. C. Wang, M. J. Powell, V. M. Popov, R. G. Pestell, Acetylation in nuclear receptor signaling and the role of sirtuins. *Mol Endocrinol* **22**, 539-545 (2008).
36. X. Corso-Díaz *et al.*, Co-activator candidate interactions for orphan nuclear receptor NR2E1. *BMC Genomics* **17**, 832 (2016).
37. D. Bustos, C. E. Bakalarski, Y. Yang, J. Peng, D. S. Kirkpatrick, Characterizing ubiquitination sites by peptide-based immunoaffinity enrichment. *Mol Cell Proteomics* **11**, 1529-1540 (2012).
38. V. V. Courouble *et al.*, Revealing the Structural Plasticity of SARS-CoV-2 nsp7 and nsp8 Using Structural Proteomics. *J Am Soc Mass Spectrom* **32**, 1618-1630 (2021).